

## Efficient Perovskite Solar Cells Prepared by Hot Air Blowing Ultrasonic Spraying in Ambient Air

Jian Su, Hongkun Cai, Xiaofang Ye, Xiaojun Zhou, Jingtao Yang, Dan Wang, Jian Ni, Juan Li, and Jianjun Zhang

*ACS Appl. Mater. Interfaces*, **Just Accepted Manuscript** • DOI: 10.1021/acsami.9b01843 • Publication Date (Web): 25 Feb 2019

Downloaded from <http://pubs.acs.org> on February 27, 2019

### Just Accepted

“Just Accepted” manuscripts have been peer-reviewed and accepted for publication. They are posted online prior to technical editing, formatting for publication and author proofing. The American Chemical Society provides “Just Accepted” as a service to the research community to expedite the dissemination of scientific material as soon as possible after acceptance. “Just Accepted” manuscripts appear in full in PDF format accompanied by an HTML abstract. “Just Accepted” manuscripts have been fully peer reviewed, but should not be considered the official version of record. They are citable by the Digital Object Identifier (DOI®). “Just Accepted” is an optional service offered to authors. Therefore, the “Just Accepted” Web site may not include all articles that will be published in the journal. After a manuscript is technically edited and formatted, it will be removed from the “Just Accepted” Web site and published as an ASAP article. Note that technical editing may introduce minor changes to the manuscript text and/or graphics which could affect content, and all legal disclaimers and ethical guidelines that apply to the journal pertain. ACS cannot be held responsible for errors or consequences arising from the use of information contained in these “Just Accepted” manuscripts.



# Efficient Perovskite Solar Cells Prepared by Hot Air Blowing Ultrasonic Spraying in Ambient Air

*Jian Su<sup>1,2</sup>, Hongkun Cai<sup>1,2\*</sup>, Xiaofang Ye<sup>1,2</sup>, Xiaojun Zhou<sup>1,2</sup>, Jingtao Yang<sup>1,2</sup>, Dan Wang<sup>1,2</sup>, Jian Ni<sup>1, 2\*</sup>, Juan Li<sup>1, 2</sup>, Jianjun Zhang<sup>1,2</sup>*

1. Department of Electronic Science and Technology, College of Electronic Information and Optical Engineering, Nankai University, Tianjin, 300350, China
2. Key Laboratory of Photoelectronic Thin Film Devices and Technology of Tianjin, Tianjin, 300350, China

## Corresponding Author

\*E-mail: [caihongkun@nankai.edu.cn](mailto:caihongkun@nankai.edu.cn); [nijian\\_nankai@163.com](mailto:nijian_nankai@163.com)

**KEYWORDS:** ultrasonic spray coating, substrate heating, hot air blowing, perovskite solar cells, scalable atmospheric deposition

1  
2  
3  
4 **ABSTRACT :** Substrate heating is the most common method for controlling crystallization  
5  
6 during spray coating. However, due to poor controllability during substrate heating, the sprayed  
7  
8 films have variable thickness and rich pores, which limits the efficiency of the device. Here, hot  
9  
10 air blowing was applied to spray coating to promote the crystallization of perovskite films under  
11  
12 ambient conditions. Upon employing a hot air blowing method that stimulated uniformly  
13  
14 distributed nuclei growth, the pinhole-free and thickness-controllable perovskite film was prepared.  
15  
16  
17 This enabled more reproducibly high quality perovskite films to achieve power conversion  
18  
19 efficiency (PCE) of 13.5% and obtain stabilized power output (SPO) of >12% in ambient  
20  
21 conditions.  
22  
23  
24  
25  
26  
27  
28  
29  
30  
31  
32  
33  
34  
35  
36  
37  
38  
39  
40  
41  
42  
43  
44  
45  
46  
47  
48  
49  
50  
51  
52  
53  
54  
55  
56  
57  
58  
59  
60

## INTRODUCTION

Hybrid organic-inorganic perovskite has arisen as a revolutionary absorber material due to its excellent photoelectric properties. The PCE of perovskite solar cell (PSC) has exceeded 23% in only a few years<sup>1-8</sup>. However, the commercialization of PSC requires not only high PCE but also scalability and stability. Spin coating is the most commonly used perovskite film deposition techniques. In the spin coating process, the drying and flattening of wet films depend on the successive centripetal force generated by rotation. Unfortunately, spin coating is difficult to apply to the preparation of scalable perovskite films. This area of the substrate is always less than 10 cm, and most of the precursor ink (> 90%) was wasted in spin coating process<sup>9</sup>. Therefore, developing scalable perovskite film deposition methods and understanding the film formation mechanism are the key to improve the scalability of PSC devices.

Developing a suitable deposition strategy for expandable perovskite absorbing layer is a challenge for expanding perovskite solar cell devices. The technologies for scalable perovskite film deposition include blade coating<sup>10-12</sup>, slot-die coating<sup>13-14</sup>, meniscus coating<sup>15</sup>, spray coating<sup>16-21</sup>, inkjet printing<sup>22-23</sup>, screen printing<sup>24-25</sup> and electrodeposition<sup>26-30</sup>. Spray coating which can be easily scaled up and translated to roll-to-roll fabrication is a fascinating technology to meet the commercialization of PSCs. There are many examples of depositing compact oxide by pneumatic spraying<sup>31</sup> and ultrasonic spraying<sup>32</sup>. Ultrasonic spray coating (USC) could also be used to deposit perovskite absorbing layer<sup>19, 21</sup>. Previous works have focused on the substrate heating method<sup>17-18</sup> and the growth mechanism of perovskite films in ultrasonic spray coating<sup>16</sup>. By optimizing substrate temperature which could affect the perovskite films quality, the PSC devices with an

1  
2  
3  
4 average efficiency of  $10.6 \pm 1.1\%$  were obtained at  $75^\circ\text{C}$ <sup>17</sup>. The most efficient (18.3%) sprayed  
5  
6 PSC device was fabricated at  $120^\circ\text{C}$  of substrate temperature<sup>20</sup>. It is not easy to maintain the  
7  
8 delicate balance of solvent evaporation and crystallization speed by tuning the substrate  
9  
10 temperature. In the previous report of Zhu et al., PCE of 17.29% was obtained for the application  
11  
12 of antisolvent which is environmentally harmful<sup>33</sup>. Therefore, a more controllable method was  
13  
14 urgently needed to prepare dense uniform perovskite films via spraying.  
15  
16  
17  
18

19  
20 Gas-assisting method (the gas was usually high-pressure inert gas) has been introduced to spin  
21  
22 coating<sup>34-36</sup>, but almost no ultrasonic spray coating. Here, we firstly applied a hot air blowing  
23  
24 method to ultrasonic spray coating under ambient conditions ( $\text{RH} < 30\%$ ). Good reproducible  
25  
26 pinhole-free perovskite films were prepared by hot air blowing ultrasonic spray coating (HAB-  
27  
28 USC) rather than substrate heating ultrasonic spray coating (SH-USC). The time and temperature  
29  
30 of air flow have been optimized to pursue pinhole-free perovskite films. The planer PSC devices  
31  
32 were achieved with PCE of 13.5% ( $0.13 \text{ cm}^2$ ) and 9.80% ( $1 \text{ cm}^2$ ). The HAB-USC PSC devices  
33  
34 were more efficient and stable, and the method of HAB-USC played a key role in low cost and  
35  
36 high throughput manufacturing of PSC devices.  
37  
38  
39  
40  
41  
42

## 43 **EXPERIMENTAL**

44  
45 **Materials and Solution Preparation.** The precursor solution of electron transport layer was  
46  
47 obtained by mixing 1 ml of tin oxide colloidal dispersion (Alfa Aesar, 15% in  $\text{H}_2\text{O}$  colloidal  
48  
49 dispersion) and 5 ml of deionized water and then stirring 2 hours.  
50  
51  
52  
53  
54  
55  
56  
57  
58  
59  
60

1  
2  
3  
4 The  $\text{CH}_3\text{NH}_3\text{PbI}_{3-x}\text{Cl}_x$  precursor solution was obtained by blending  $\text{PbCl}_2$  (99.999%, Sigma-  
5  
6 Aldrich) and MAI (> 99.5%, Shanghai Materwin New Materials Co. Ltd.) in a molar ratio of 1:3  
7  
8 in anhydrous DMF.  
9

10  
11 The hole transport layer precursor solution was obtained following a recipe published  
12 elsewhere<sup>33</sup>. Spiro-OMeTAD (99.5%), Li-TFSI and FK-209 were all purchased from Shanghai  
13  
14 Zaofu New Material Technology Co., Ltd. 4-tBP was purchased from Sigma-Aldrich.  
15  
16  
17

18  
19 **Perovskite Film Deposition.** For spray coating, 450 mg/ml  $\text{CH}_3\text{NH}_3\text{PbI}_{3-x}\text{Cl}_x$  precursor  
20  
21 solution was used. The perovskite precursor solution that was delivered by the Syringe Pump  
22  
23 (LSP01-1A, Longer Precision Pump Co., Ltd) was sprayed in ambient air by a self-built spray  
24  
25 system equipped with a 120 kHz nozzle (K12, Siansonic Technology Co., Ltd). The perovskite  
26  
27 films were prepared with the optimized ultrasonic spraying parameters: a nozzle height of 80 mm,  
28  
29 a flow rate of 2.0 ml/min, a substrate moving speed of 100 mm/s (driven by a stepper motor), and  
30  
31 a carrier gas pressure of 4.4 psi.  
32  
33  
34  
35  
36

37 For conventional SH-USC, we have preheated the substrate with different temperature. To keep  
38  
39 the substrate at a specific temperature during the whole deposition process, we fixed the substrate  
40  
41 on a 10 cm × 10 cm aluminum plate which has high specific heat capacity before preheating. After  
42  
43 15 minutes preheated of glass substrate and aluminum plate, the substrate fixed on aluminum plate  
44  
45 was transferred to the spray system for spray coating. The annealing process was 30 minutes at  
46  
47 90°C for and 60 minutes at 100°C in ambient atmosphere.  
48  
49  
50  
51

52  
53 For novel HAB-USC, the as-prepared substrate passed directly under the nozzle and then hot air  
54  
55 was applied to the wet film. The hot air of specific temperature was provided by digital display  
56  
57

1  
2  
3  
4 hot air heat gun (DHCHG11600, DELIXI ELECTRIC). The distance between wet films and heat  
5  
6 gun orifice was 30 mm and the flow rate of hot air was 8 liters/sec. The temperature of hot air in  
7  
8 this work shown on the digital display screen of the heat gun. Thermal annealing process of  
9  
10 perovskite film was the same as SH-USC mentioned above.  
11  
12

13  
14 **Solar Cell Device Fabrication.** For the rigid substrate, ITO/glass (Nippon, 10  $\Omega$ /sq) was  
15  
16 washed 15 min by sonication in deionized water, ethanol and acetone, respectively. The ITO-  
17  
18 coated glass was dealt with ultraviolet ozone (UVO) for 15 min before using after drying by N<sub>2</sub>  
19  
20 stream. SnO<sub>2</sub> layer was spin coated at 3000 rpm for 30 s and then annealed at 150°C for half an  
21  
22 hour in ambient air. Then SnO<sub>2</sub>/ITO/glass was dealt with UVO for 15 min before depositing  
23  
24 perovskite precursor solution.  
25  
26  
27  
28

29  
30 For the flexible substrate, ITO/PEN (Pecell Technologies, Inc., 15  $\Omega$ /sq) was only cleaned 15  
31  
32 min by sonication in deionized water and then was further dealt with UVO treatment for 10 min  
33  
34 before use. The deposition and annealing process of SnO<sub>2</sub> on the flexible substrate as same as on  
35  
36 ITO/glass. Then the SnO<sub>2</sub>/ITO/PEN substrate was dealt with UVO treatment for 10 min before  
37  
38 spray coating.  
39  
40  
41

42  
43 Spiro-OMeTAD was deposited onto sprayed perovskite film prepared by aforementioned USC  
44  
45 methods at 4000 rpm for 30 s in glovebox filled with Nitrogen. Finally 80nm Au electrode was  
46  
47 thermal evaporated with a shadow mask (0.13 cm<sup>2</sup> and 1 cm<sup>2</sup>) to complete the devices.  
48  
49

50  
51 **Measurements and Characterization.** The film morphology was carried out by scanning  
52  
53 electron microscope (JSM-7800), optical microscope (Photoelectric Technology Co. Ltd,  
54  
55 UMT203i) and atomic force microscope (Bruker Dimension Icon). X-ray diffraction was given by  
56  
57

1  
2  
3  
4 Rigaku Smart Lab with a Cu K $\alpha$  source. *J-V* curves of the PSC cells were measured at a delay time  
5  
6 of 100 ms by Keithley 2611 source meter at room environment. There was no initial light soaking.  
7  
8  
9 The light source was a solar simulator (Newport, 81904, USA) under the AM 1.5G (100 mW/cm<sup>2</sup>),  
10  
11 which was calibrated by a standard Si cell. Electrochemical impedance spectroscopy (EIS)  
12  
13 measurement of PSC device was carried out using the electrochemical lab (AMETEK, Versa  
14  
15 STAT 4). The Nyquist plots of these devices were carried out under AM 1.5G with an applied bias  
16  
17 voltage of 10 mV.  
18  
19  
20  
21

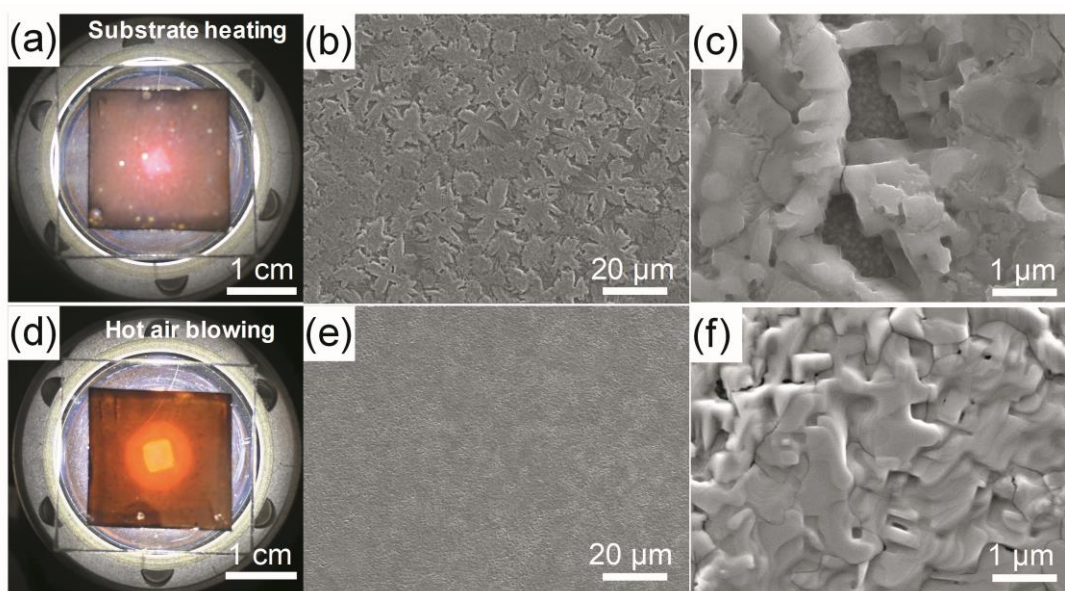
## 22 **RESULTS AND DISCUSSION**

23

24  
25 Ultrasonic spray coating had many technical parameters affecting the quality of perovskite films,  
26  
27 including but not limited to the height of the nozzle, the concentration and flow rates of perovskite  
28  
29 precursor solution, the pressure of the carrier gas and the speed of the substrate. To prepare  
30  
31 perovskite films with a one-step spray coating method, we have set up an ultrasonic spraying  
32  
33 system in our lab. The parameters mentioned above have been optimized carefully, and specific  
34  
35 parameters have been introduced in the experimental section. It was worth mentioning that  
36  
37 multiple pass spray routines could redissolve the underlying films resulting in poor quality of  
38  
39 perovskite films. Therefore, single pass spray routine is imperative (Figure S1).  
40  
41  
42  
43  
44

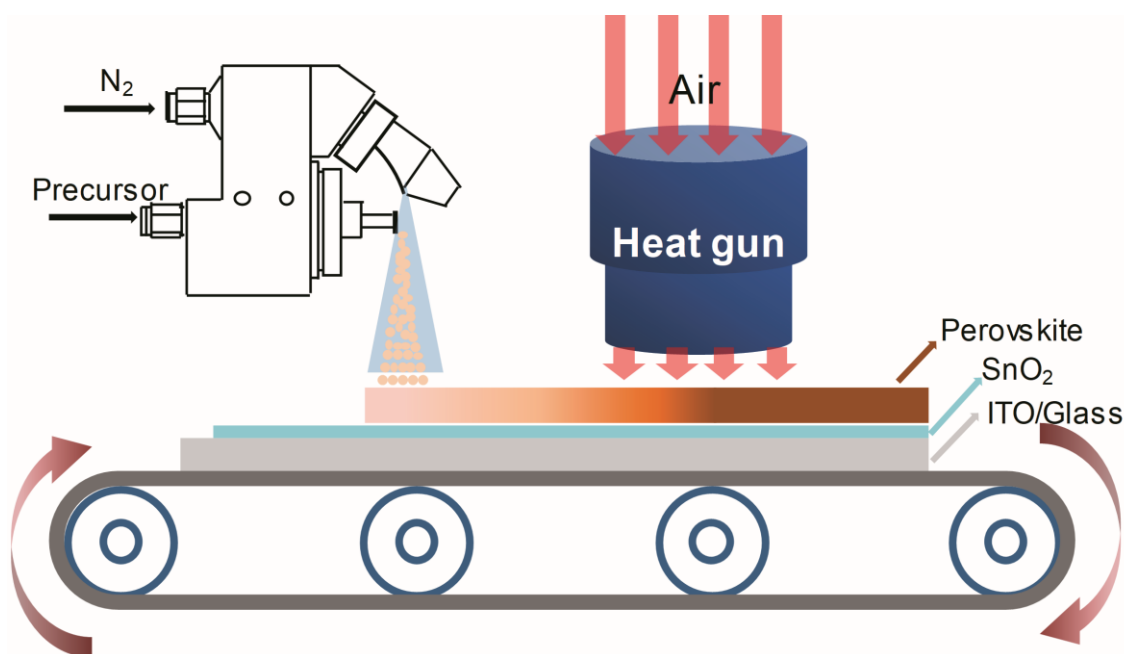
45  
46 The solution deposition methods of perovskite films all contain three key stages: i) the coating  
47  
48 of wet precursor film and coalescence of droplets, ii) the evaporation of solvent and nucleation, iii)  
49  
50 the crystallization of perovskite by annealing. In ultrasonic spray coating, tiny liquid droplets were  
51  
52 randomly dispersed onto the substrate with the assistance of carrier gas. It was easy to coat  
53  
54 perovskite precursor solution onto the substrate via ultrasonic spray coating, and thermal annealing  
55  
56  
57  
58  
59  
60

1  
2  
3  
4 to crystallize fully the perovskite film was already a mature technology for  $\text{CH}_3\text{NH}_3\text{PbI}_{3-x}\text{Cl}_x$  films.  
5  
6  
7 The second stage of solvent evaporation was the most critical factor in the process of perovskite  
8  
9 film deposition. In the existing reports<sup>16-21</sup>, almost sprayed perovskite films were prepared by SH-  
10  
11 USC, which the solvent evaporation rate was controlled by the substrate heating method. However,  
12  
13 the optimized temperatures are varied in different reports<sup>16-18</sup>. We firstly prepared perovskite films  
14  
15 with different substrate temperature by SH-USC. Figure S2 shown that the films prepared by  
16  
17 relative lower temperature process exhibited irregularly distributed flower-like shaped crystal  
18  
19 because of the de-wetting resulted from prolonged drying time. Moreover, the films prepared by  
20  
21 relative higher temperature process exhibited lower film coverage and high roughness, because the  
22  
23 solvent evaporated too quickly to coalesce the droplets, even the solvent would vaporize  
24  
25 immediately upon touching the hot plate.  
26  
27  
28  
29  
30  
31



32  
33  
34  
35  
36  
37  
38  
39  
40  
41  
42  
43  
44  
45  
46  
47  
48  
49  
50  
51  
52  
53 **Figure 1.** Digital photos and different magnification SEM images of (a-c) SH-USC perovskite  
54  
55 film, (d-f) HAB-USC perovskite film.  
56

1  
2  
3  
4 The optimal temperature was 50°C with the SH-USC method since the temperature resulted in  
5 better coverage films (Figure S2). Indeed, it was apparent that there were still relatively small holes  
6 and exposed underlying oxide (Figure 1a-c). This revealed that the high quality perovskite films  
7 and exposed underlying oxide (Figure 1a-c). This revealed that the high quality perovskite films  
8 could hardly be obtained by SH-USC. Predictably, the devices with poor coverage perovskite films  
9 would have a poor efficiency.  
10  
11  
12  
13  
14  
15



38 **Figure 2.** Schematic illustration of the HAB-USC process.

39  
40  
41 For high quality perovskite films, a novel method named hot air blowing ultrasonic spray coating  
42 was developed. Figure 2 illustrated the HAB-USC process that we employed hot air blowing to  
43 deposit  $\text{CH}_3\text{NH}_3\text{PbI}_{3-x}\text{Cl}_x$  films. The precursor ink was transported into the ultrasonic nozzle by a  
44 micro syringe pump, and broken into micron droplets by nozzle vibrating. Under the guidance of  
45 carrier gas ( $\text{N}_2$ ), a perovskite precursor wet-film was spray-coated onto the substrate of  $\text{SnO}_2/\text{ITO}$ .  
46  
47  
48  
49  
50  
51  
52  
53  
54 To ensure the continuity of the preparation process, the substrate was driven by a stepped motor  
55  
56  
57  
58  
59  
60

1  
2  
3  
4 to pass through directly under the ultrasonic nozzle at a speed of 100 mm/s. After a few seconds  
5  
6 (to ensure coalescence of droplets), hot air was used to blow the perovskite precursor wet-films to  
7  
8 adjust the evaporation of the solvent. It was worth mentioning that our USC system achieved  
9  
10 deposition speed one order of magnitude larger than blade coating (which typically was 1–13  
11  
12 mm/s<sup>10-12</sup>). Amazingly, upon employing hot air blowing to the preparation process of perovskite  
13  
14 films, pinhole-free perovskite films were obtained (Figure 1d-f). Therefore, the HAB-USC method  
15  
16 we have developed provided a new opportunity for obtaining high-quality perovskite films even  
17  
18 capturing high-efficiency devices.  
19  
20  
21  
22  
23

24  
25 As discussed above, the second stage of solvent evaporation and nucleation was the decisive  
26  
27 factor for high quality perovskite films. For the conventional SH-USC process, we need to increase  
28  
29 the temperature of the hot plate to accelerate the evaporation of solvent due to low temperature  
30  
31 would cause serious dewetting. When the perovskite precursor solution was just contacted with  
32  
33 the hot plate with higher temperature, supersaturating was formed immediately because of the fast  
34  
35 evaporation of the solvent. The formation of fast-supersaturated state caused rapid accumulation  
36  
37 of solute, resulting in uneven nucleation (Figure 3a). Therefore, the substrate-heating method could  
38  
39 hardly obtain perovskite films without pinholes whether it was high or low temperature, as shown  
40  
41 in Figure S2. However, the method of HAB-USC could promote the regulation of solvent  
42  
43 evaporation rate resulting in uniform nucleation by suppressing dewetting and ultrafast-  
44  
45 supersaturated (Figure 3b). In HAB-USC, the coalescence of micro-droplets before hot air blowing  
46  
47 guaranteed the full coverage of the substrate surface. Through further hot air treatment, the solvent  
48  
49  
50  
51  
52  
53  
54  
55  
56  
57  
58  
59  
60

evaporated at suitable rates, resulting in evenly nucleation and finally dense perovskite films without pinholes.

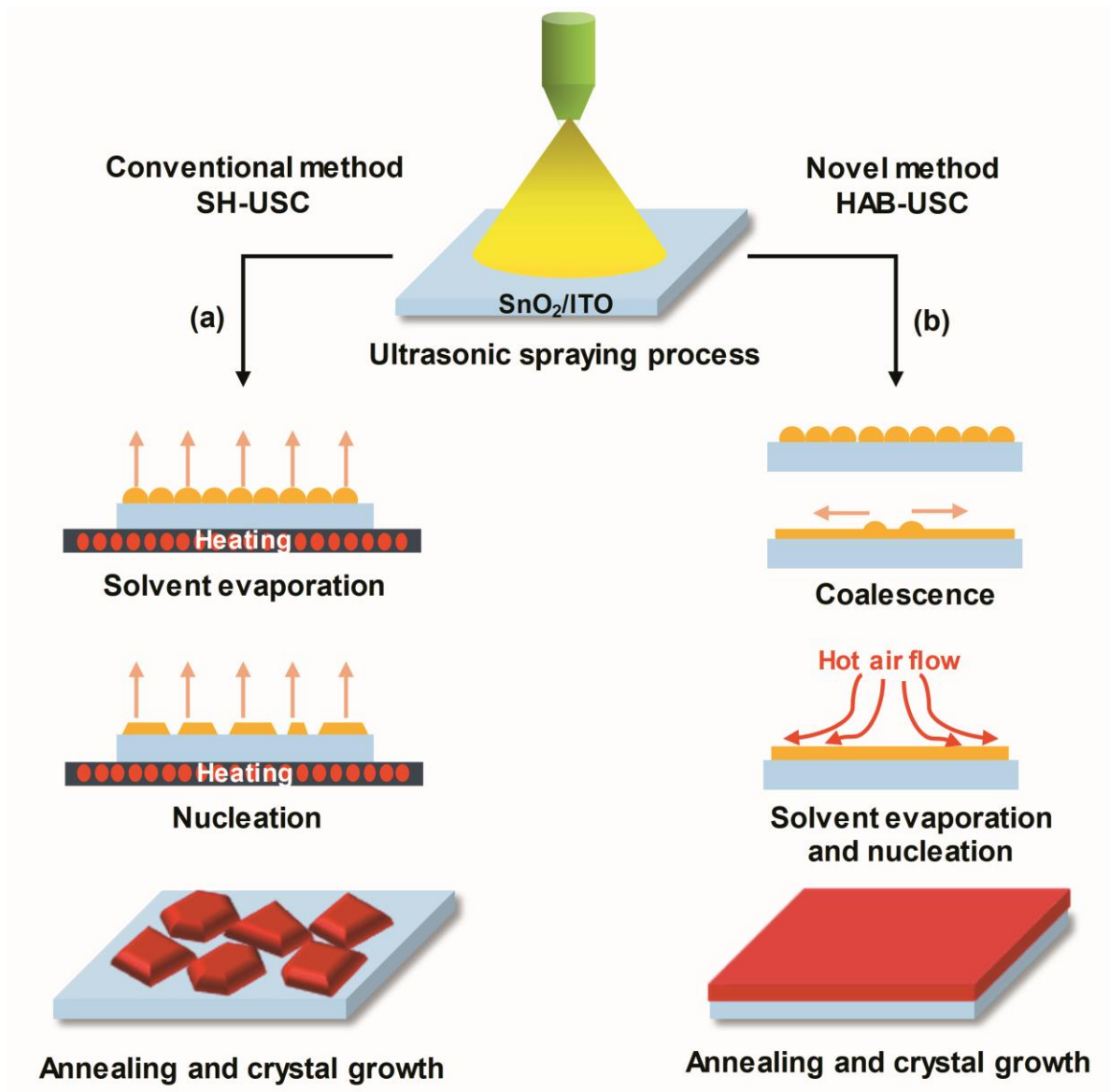


**Figure 3.** Schematic illustration of the growth of perovskite films fabricated by (a) conventional method of SH-USC and (b) novel method of HAB-USC.

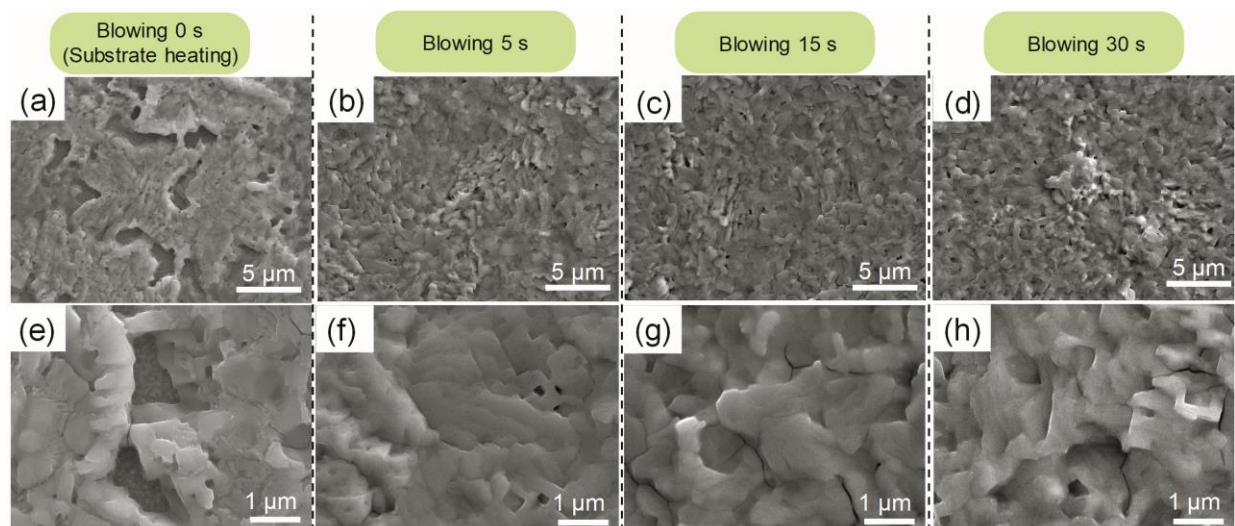


**Figure 4.** (a-d) Low magnification and (e-h) high magnification SEM images of  $\text{CH}_3\text{NH}_3\text{PbI}_{3-x}\text{Cl}_x$  films with different hot air blowing time. (Especially, the film of blowing 0 s was prepared by 50°C substrate heating ultrasonic spray coating.)

To further optimize the method of HAB-USC and explore the effect of hot air blowing on the morphology of  $\text{CH}_3\text{NH}_3\text{PbI}_{3-x}\text{Cl}_x$  films, we have employed different air blowing time and temperature to deal with the perovskite wet-films. As shown in Figure S3, we achieved uniform and dense perovskite films and the optimal temperature was 120°C with blowing time of 15 s. Figure 4 shown SEM images of  $\text{CH}_3\text{NH}_3\text{PbI}_{3-x}\text{Cl}_x$  films under different hot air blowing time at 120°C. Figure S4 and S5 shown good crystallinity of all perovskite films, which could attribute to suitable post-annealing treatment and appropriate humidity (RH 20% - 30%). Exceptionally, Figure S4 shown that the films with a higher temperature ( $\geq 130^\circ\text{C}$ ) substrate heating were splitting due to the formation of smaller grain (Figure S2). As shown in Figure 4a and 4e, hole-rich perovskite films were obtained when perovskite wet-films were blown 0 s (the sample was treated with substrate heating of 50°C which is the optimized temperature of substrate heating). Especially

when hot air was applied to the wet-films, the coverage of perovskite films increased significantly even after 5 s hot air treatment.

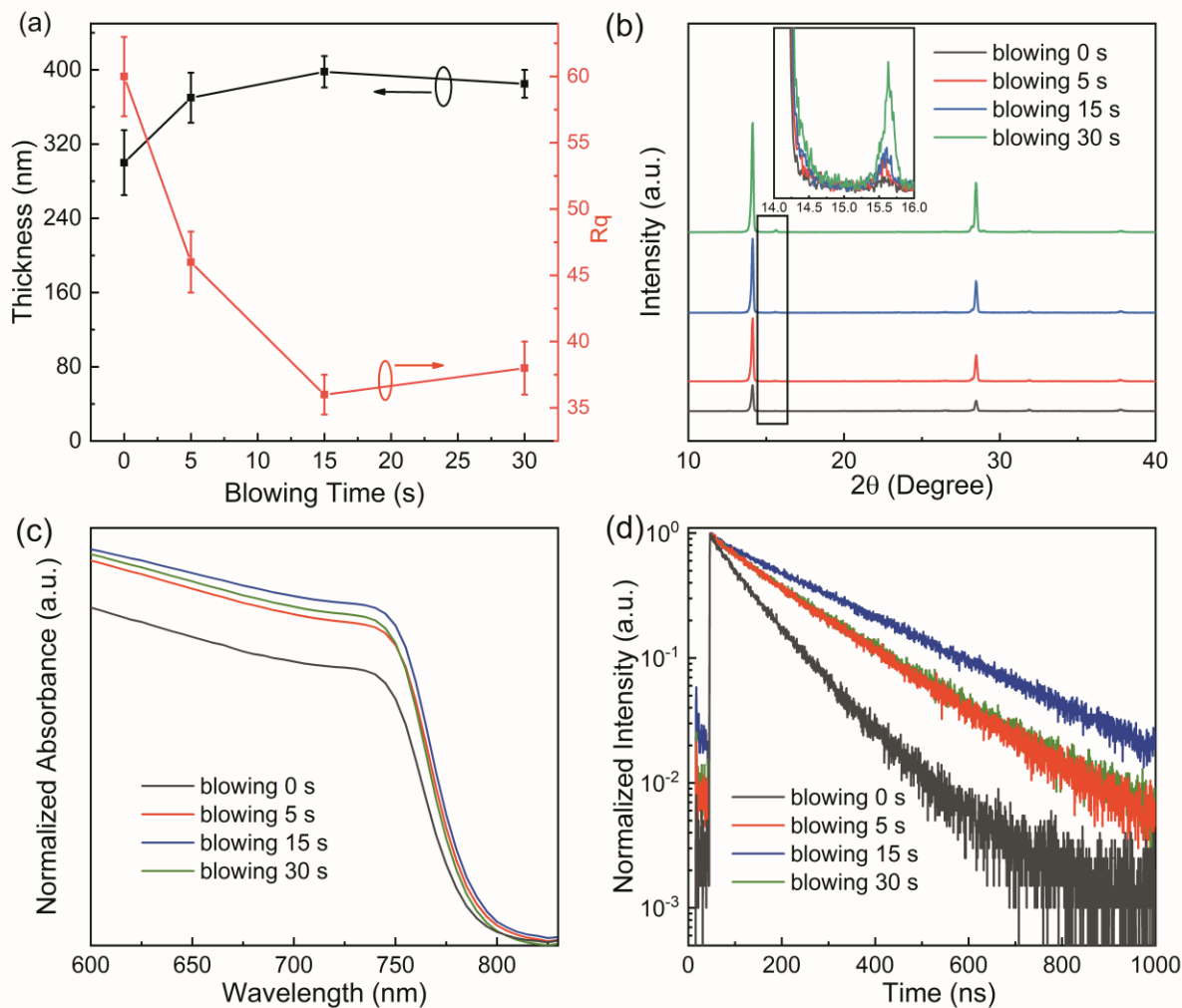


**Figure 5.** (a) Thickness and RMS of  $\text{CH}_3\text{NH}_3\text{PbI}_{3-x}\text{Cl}_x$  films. (b) XRD patterns of  $\text{CH}_3\text{NH}_3\text{PbI}_{3-x}\text{Cl}_x$  films. (c) Absorption spectra (glass/ $\text{CH}_3\text{NH}_3\text{PbI}_{3-x}\text{Cl}_x$ ). (d) Time resolved photoluminescence spectroscopy (TRPL) for  $\text{CH}_3\text{NH}_3\text{PbI}_{3-x}\text{Cl}_x$  films with different blowing time.

However, the perovskite films have the best morphology and optical performance when the hot air blowing time was 15 s. Figure 5a shown the roughness of the perovskite films decreased firstly

1  
2  
3  
4 and then increased as increasing the blowing time to 30 s. We made the film thickness controllable  
5  
6 by adjusting the precursor flow rates at a fixed substrate speed. Figure S6b shows the good liner  
7  
8 relationship between perovskite thickness and precursor flow rates at a fixed substrate speed of  
9  
10 100 mm/s. The thickness of perovskite films was measured by the step measurement method of  
11  
12 AFM that was introduced in Figure S7. The thickness of perovskite films with different hot air  
13  
14 blowing time was similar (360 nm ~ 400 nm) and apart from the sample without blowing. Figure  
15  
16 5b shown the films acquired sharp and strong XRD diffraction peaks. With the increase of hot air  
17  
18 blowing time, the intensity of the Bragg diffraction peak increased too. The molar ratio of  $\text{PbCl}_2$   
19  
20 and  $\text{CH}_3\text{NH}_3\text{I}$  in  $\text{CH}_3\text{NH}_3\text{PbI}_{3-x}\text{Cl}_x$  perovskite precursor solution was pivotal to the phase purity  
21  
22 of annealed perovskite films. The increased blowing time of hot air led to the deviation of the  
23  
24 molar ratio of perovskite precursor solution because of the volatilization of organic components  
25  
26 ( $\text{CH}_3\text{NH}_3\text{I}$ ). The perovskite films blown 30 s exhibited increased intensity of  $\text{CH}_3\text{NH}_3\text{PbCl}_3$  peak  
27  
28 at  $15.6^\circ$  (the inset of Figure 5b), which would inhibit the improvement of PCE. This is consistent  
29  
30 with previous reports that crystalline  $\text{CH}_3\text{NH}_3\text{PbCl}_3$  would occur in annealed  $\text{CH}_3\text{NH}_3\text{PbI}_3$   
31  
32 perovskite films if the molar ratio of  $\text{PbCl}_2$  and  $\text{CH}_3\text{NH}_3\text{I}$  deviates from 1:3<sup>37</sup>. As shown in Figure  
33  
34 5c, the films blown 15 s obtained stronger absorption because of the larger thickness shown in  
35  
36 Figure 5a. Time resolved photoluminescence spectroscopy (TRPL) shown increased PL lifetimes  
37  
38 of perovskite film blown 15 s, revealing elevated film quality and reduced traps. This was essential  
39  
40 for high performance because of the suppression of non-radiative recombination pathways (Figure  
41  
42 5d).  
43  
44  
45  
46  
47  
48  
49  
50  
51  
52  
53  
54  
55  
56  
57  
58  
59  
60

**Table 1.** PV parameters of spray-coated PSCs with different hot air blowing time. <sup>a</sup>

Blowing Time (s)	$J_{sc}$ (mA/cm <sup>2</sup> )	$V_{oc}$ (V)	FF (%)	PCE (%)
0	10.97 ± 1.18	0.747 ± 0.049	54.3 ± 4.2	4.46 ± 0.73
5	16.44 ± 0.76	0.841 ± 0.029	58.2 ± 2.9	8.04 ± 0.53
15	18.17 ± 0.65	0.932 ± 0.048	65.5 ± 3.7	11.12 ± 1.05
30	17.24 ± 0.36	0.886 ± 0.029	62.8 ± 2.2	9.59 ± 0.45

<sup>a</sup> 64 cells were fabricated in four batches.

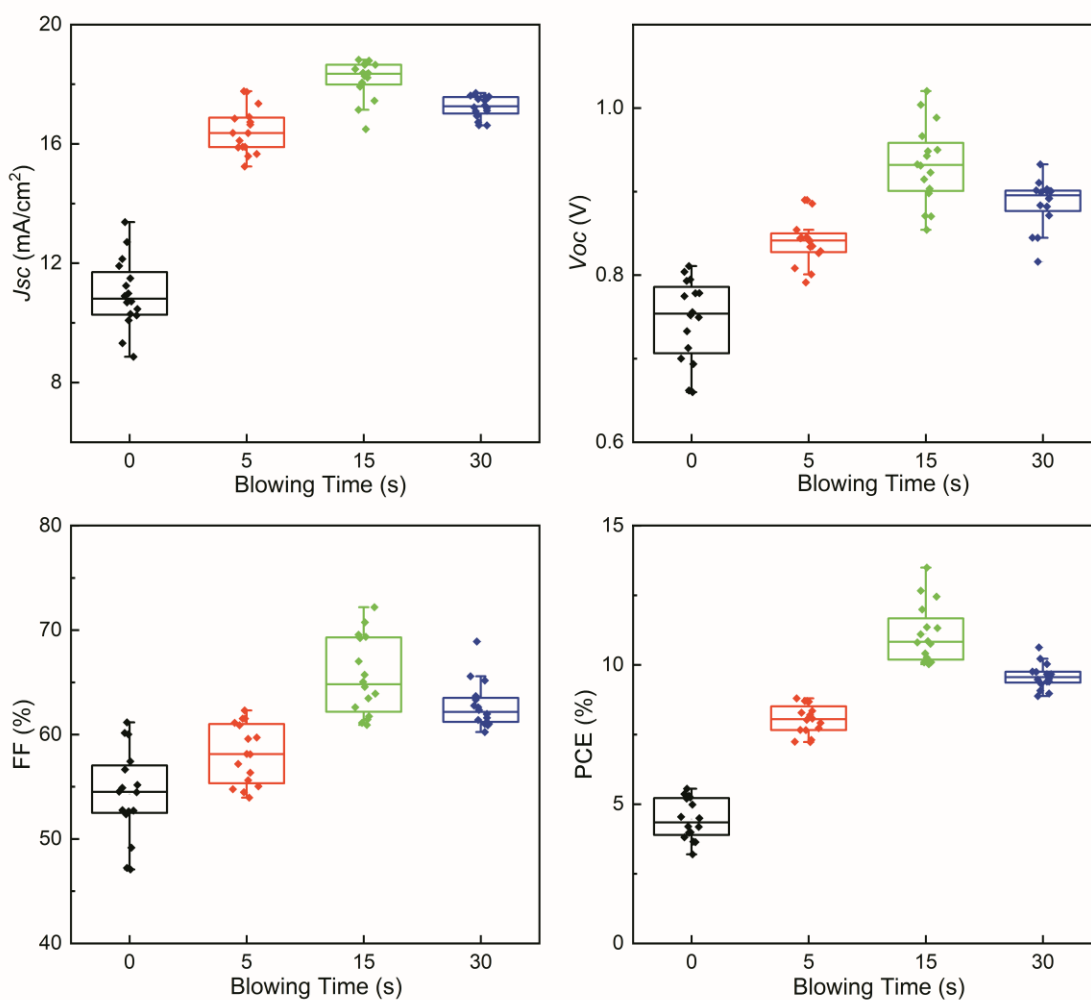


**Figure 6.** Statistical results of 64 devices in different batches treated by different hot air blowing time.

Table 1 summarized the average and standard deviation of the PV parameters of 64 devices. Figure 6 shown the device statistics of 64 devices (16 devices for each different blowing time) collected from 4 batches. With the blowing time increasing from 0 s to 15 s, all parameters had increased and  $11.12 \pm 1.05\%$  of average PCE was achieved when blowing time was 15 s. Compared with PSCs blown 15 s, these devices blown 30 s had lower  $J_{sc}$  and  $V_{oc}$  because of the impurity phase.

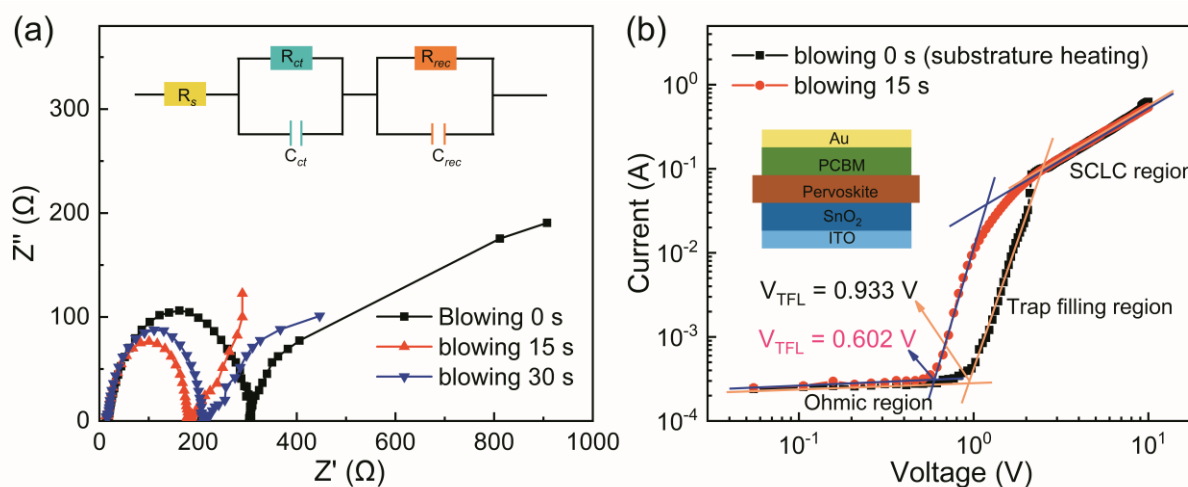


**Figure 7.** (a) The typical Nyquist plots of PSCs. (b) Dark  $J$ - $V$  curves of electron-only devices of hot air blowing 0 s and 15 s.

The measurement of EIS is a commonly used characterization method that indicates the carrier transport behavior in PSC devices<sup>38</sup>. The Nyquist plots of these devices were carried out under AM 1.5G with an applied bias voltage of 10 mV as shown in Figure 7a. The inside illustration of Figure 7a was the equivalent circuit. There were semicircles which were located at high frequency ranges and lines which were located at low frequency. Normally, the low frequency region represents charge recombination resistance ( $R_{rec}$ ), which the high frequency region indicates

1  
2  
3  
4 charge transport resistance ( $R_{ct}$ ). So EIS data showed the improved charge transport in PSCs with  
5  
6 perovskite of hot air blowing 15 s. At the same time, higher  $R_{rec}$  exposed smaller recombination  
7  
8 which was consistent with TRPL conclusions. On account of poor phase purity, the film blown 15  
9  
10 s exhibited higher  $R_{rec}$  than 30 s, which indicated that the film blown 15 s had higher recombination.  
11  
12  
13

14 The dark current was associated with the trap density. The electron trap density was calculated  
15  
16 from the dark J-V curve of the electron-only device which have a structure of  
17  
18 ITO/SnO<sub>2</sub>/Perovskite/PCBM/Au (Figure 7b). There were Ohmic region, trap filling region and  
19  
20 space charge limited current region. The trap density ( $N_d$ ) was determined by the voltage at which  
21  
22 all the traps filled (trap-filled limit voltage  $V_{TFL}$ )<sup>39</sup>:  
23  
24  
25

$$V_{TFL} = eN_dL^2/2\epsilon\epsilon_0 \quad (1)$$

26  
27 where  $e$  presents elementary charge,  $L$  presents the thickness of CH<sub>3</sub>NH<sub>3</sub>PbI<sub>3-x</sub>Cl<sub>x</sub> film (Figure  
28  
29 S8),  $\epsilon$  (=32)<sup>39</sup> indicates relative dielectric constant,  $\epsilon_0$  indicates vacuum dielectric constant. The  
30  
31 trap density in PSCs with hot air blowing was calculated to be  $1.3 \times 10^{-16} \text{ cm}^{-3}$ , which is smaller  
32  
33 than the PSCs without hot air blowing ( $3.3 \times 10^{-16} \text{ cm}^{-3}$ ). The elevated trap density could be ascribed  
34  
35 to the higher quality of the CH<sub>3</sub>NH<sub>3</sub>PbI<sub>3-x</sub>Cl<sub>x</sub> films induced from hot air blowing.  
36  
37  
38  
39  
40  
41  
42  
43  
44  
45  
46  
47  
48  
49  
50  
51  
52  
53  
54  
55  
56  
57  
58  
59  
60

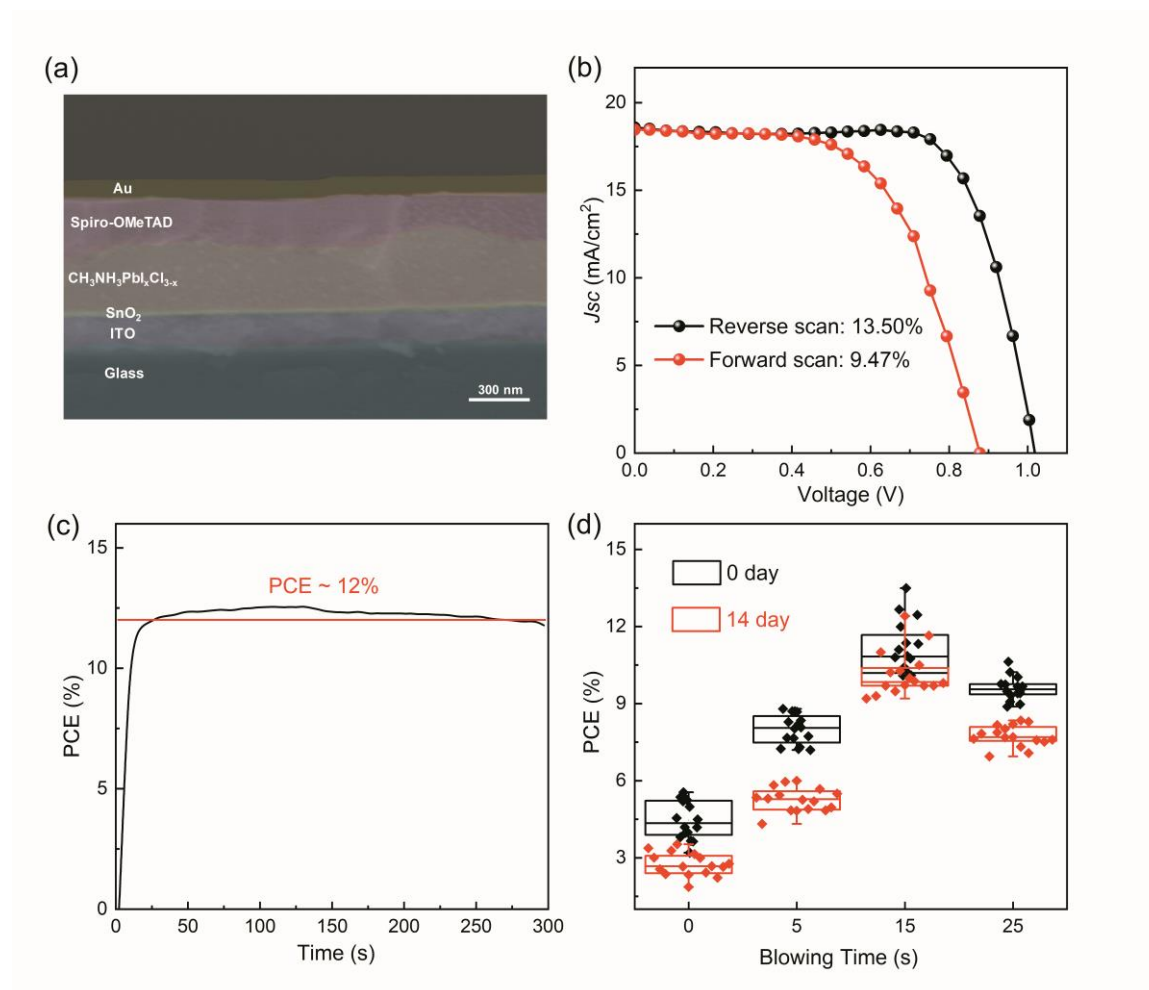


**Figure 8.** (a) Cross-sectional SEM image of spray-coated cell. (b)  $J$ - $V$  curves with different scan direction of champion cell. (c) Stabilized power output test of champion cell. (d) Statistical results of PSC devices performance on 0 day and 14 day (stored in ambient air,  $T$ : 20~25°C,  $RH$ : 20~30%).

Figure 8a shown the cross-sectional SEM images of spray-coated cell. Figure 8b shown the different scan direction  $J$ - $V$  curves of the champion device obtained by 15 s HAB-USC (Figure S9 shown the corresponding EQE). There was severe hysteresis which could be ascribed to misaligned conduction band between  $\text{CH}_3\text{NH}_3\text{PbI}_{3-x}\text{Cl}_x$  and  $\text{SnO}_2$ <sup>40</sup>. Compared with the spin-coated spiro-OMeTAD and  $\text{SnO}_2$ , the perovskite films prepared by spray coating have higher

roughness, resulting in poor interface<sup>33</sup>. The difference of charge transport ability between charge collection layer and perovskite layer generally attributed to more pronounced hysteresis<sup>41</sup>. Some studies have shown that adding [6,6]-phenyl-C61-butyric acid methyl ester (PCBM) into the interface of SnO<sub>2</sub> and perovskite layer could reduce hysteresis and increase PCE<sup>42</sup>. Figure 8c shown the stabilized power output (SPO) test, which applied a constant voltage of 0.77 V for 300 s under ambient air. Figure 8d shown the statistical results of the devices efficiency decay in two weeks, which indicated the PSCs blown 15 s had better long-term stability than others especially the PSCs with substrate heating (blown 0 s). The PSCs blown 15 s still maintained an initial efficiency of over 90%.

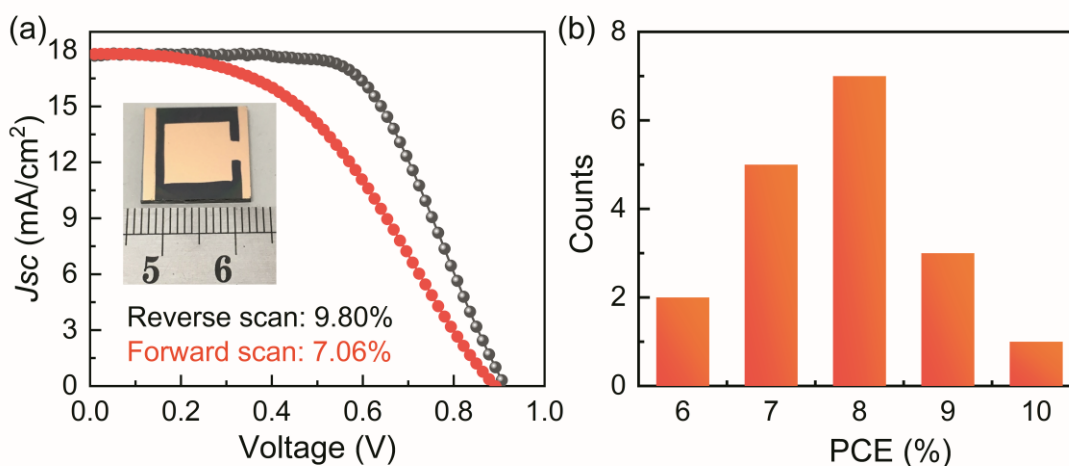


**Figure 9.** (a) The  $J-V$  curves of 1 cm<sup>2</sup> active area PSC device with glass substrate. (b) Histogram of PCEs on account of 18 cells of 1 cm<sup>2</sup> active area with rigid substrate.

To estimate scalability of the spray coating protocols, 1 cm<sup>2</sup> devices on 16 × 16 mm glass substrate have been fabricated and achieved a champion PCE of 9.80%. The corresponding  $J-V$  curves at different scanning directions and the photograph of large-area (1 cm<sup>2</sup>) were shown in

1  
2  
3  
4 Figure 9a. The lower PCE of 1 cm<sup>2</sup> devices was ascribed to the reduced open circuit voltage ( $V_{oc}$ )  
5  
6 associated with relatively inhomogeneous film on large area and the reduced fill factor (FF) due  
7  
8 to higher series resistance. Figure 9b shown a histogram of PCEs on account of 18 cells of 1 cm<sup>2</sup>  
9  
10 active area with glass substrate and clearly revealed the potential of HAB-USC in the large-scale  
11  
12 manufacturing of PSC devices. Besides, we have prepared 1 cm<sup>2</sup> PSC devices on a flexible  
13  
14 substrate (ITO/PEN). Figure S10 shown the  $J-V$  curve and photograph of 1 cm<sup>2</sup> flexible device.  
15  
16  
17 But the performance of flexible devices were unsatisfactory, and there were more questions we  
18  
19 should study deeply than that on glass substrates.  
20  
21  
22  
23

## 24 CONCLUSIONS

25  
26  
27 We successfully deposited perovskite films using a low-cost and high volume USC technique in  
28  
29 ambient atmosphere. Comparing with the method of substrate heating, the method of hot air  
30  
31 blowing made the nucleation process during solvent evaporation more controllable. After  
32  
33 optimizing the spraying conditions and hot air blowing process, the sprayed PSC devices obtained  
34  
35 a PCE of 13.50% and maintained an initial efficiency of over 90% after two weeks. At the same  
36  
37 time, large-area (1 cm<sup>2</sup>) perovskite solar cells on both glass and PEN substrate was fabricated,  
38  
39 which shown that our spraying method combined with the novel morphology-optimization strategy  
40  
41 has great potential and commercial prospects in scaling up perovskite solar cells.  
42  
43  
44  
45  
46  
47  
48

## 49 ASSOCIATED CONTENT

### 50 51 52 Supporting Information

53  
54  
55  
56 Figures S1-S10 supplied as Supporting Information.

1  
2  
3  
4 Details of optical images of  $\text{CH}_3\text{NH}_3\text{PbI}_{3-x}\text{Cl}_x$  films prepared by single pass and multiple pass  
5  
6 spray routine; SEM images and XRD pattern of perovskite films prepared by SH-USC and HAB-  
7  
8 USC; The relationship between perovskite thickness and precursor flow rates; Measurement  
9  
10 method of perovskite films thickness; Cross-sectional SEM image; External quantum efficiency  
11  
12 spectrum of champion devices; *J-V* curve of flexible PSC device.  
13  
14  
15  
16

## 17 **AUTHOR INFORMATION**

### 20 **Corresponding Author**

21  
22 \*E-mail: [caihongkun@nankai.edu.cn](mailto:caihongkun@nankai.edu.cn)  
23  
24

25  
26 \*E-mail: [nijian\\_nankai@163.com](mailto:nijian_nankai@163.com)  
27  
28  
29  
30

## 31 **ACKNOWLEDGMENT**

32  
33  
34  
35 This work was funded by the Natural Science Foundation of Tianjin City (Grant No.  
36  
37 17JCYBJC21200, 16JCYBJC16800, 18JCQNJC71800) as well as the National Natural Science  
38  
39 Foundation of China (Grant No. 61504068). We acknowledge the Fundamental Research Funds  
40  
41 for the Central Universities.  
42  
43  
44  
45  
46  
47

## 48 **REFERENCES**

49  
50  
51  
52  
53  
54  
55  
56  
57  
58  
59  
60

- 1  
2  
3  
4 (1) Kojima, A.; Teshima, K.; Shirai, Y.; Miyasaka, T. Organometal Halide Perovskites as  
5  
6 Visible-Light Sensitizers for Photovoltaic Cells. *J. Am. Chem. Soc.* **2009**, *131* (17), 6050-  
7  
8 6051.  
9  
10
- 11  
12 (2) Kim, H. S.; Lee, C. R.; Im, J. H.; Lee, K. B.; Moehl, T.; Marchioro, A.; Moon, S. J.;  
13  
14 Humphrybaker, R.; Yum, J. H.; Moser, J. E. Lead Iodide Perovskite Sensitized All-Solid-  
15  
16 State Submicron Thin Film Mesoscopic Solar Cell with Efficiency Exceeding 9%. *Sci. Rep.*  
17  
18 **2012**, *2* (8), 591.  
19  
20
- 21  
22 (3) Lee, M. M.; Teuscher, J.; Miyasaka, T.; Murakami, T. N.; Snaith, H. J. Efficient Hybrid  
23  
24 Solar Cells Based on Meso-Superstructured Organometal Halide Perovskites. *Science* **2012**,  
25  
26 *338* (6107), 643-647.  
27  
28
- 29  
30 (4) Zhou, H.; Chen, Q.; Li, G.; Luo, S.; Song, T.-b.; Duan, H.-S.; Hong, Z.; You, J.; Liu, Y.;  
31  
32 Yang, Y. Interface Engineering of Highly Efficient Perovskite Solar Cells. *Science* **2014**,  
33  
34 *345* (6196), 542-546.  
35  
36
- 37  
38 (5) Yang, W. S.; Noh, J. H.; Jeon, N. J.; Kim, Y. C.; Ryu, S.; Seo, J.; Sang, I. S. High-  
39  
40 Performance Photovoltaic Perovskite Layers Fabricated through Intramolecular Exchange.  
41  
42 *Science* **2015**, *348* (6240), 1234.  
43  
44
- 45  
46 (6) Li, X.; Bi, D.; Yi, C.; Décoppet, J. D.; Luo, J.; Zakeeruddin, S. M.; Hagfeldt, A.; Grätzel,  
47  
48 M. A Vacuum Flash-Assisted Solution Process for High-Efficiency Large-Area Perovskite  
49  
50 Solar Cells. *Science* **2016**, *353* (6294), 58-62.  
51  
52  
53  
54  
55

- 1  
2  
3  
4 (7) Yang, W. S.; Park, B. W.; Jung, E. H.; Jeon, N. J.; Kim, Y. C.; Lee, D. U.; Shin, S. S.; Seo,  
5  
6 J.; Kim, E. K.; Noh, J. H. Iodide Management in Formamidinium-Lead-Halide-Based  
7  
8 Perovskite Layers for Efficient Solar Cells. *Science* **2017**, *356* (6345), 1376-1379.  
9  
10  
11  
12 (8) National Renewable Energy Laboratory. NREL solar cell efficiency chart. *NREL*  
13  
14 [www.nrel.gov/pv/assets/images/efficiency-chart.png](http://www.nrel.gov/pv/assets/images/efficiency-chart.png) (2018).  
15  
16  
17  
18 (9) Li, Z.; Klein, T. R.; Kim, D. H.; Yang, M.; Berry, J. J.; van Hest, M. F.; Zhu, K. Scalable  
19  
20 Fabrication of Perovskite Solar Cells. *Nat. Rev. Mater.* **2018**, *3* (4), 18017.  
21  
22  
23  
24 (10) Kim, J. H.; Williams, S. T.; Cho, N.; Chueh, C. C.; Jen, A. K. Y. Enhanced Environmental  
25  
26 Stability of Planar Heterojunction Perovskite Solar Cells Based on Blade-Coating. *Adv.*  
27  
28 *Energy Mater.* **2015**, *5* (4), 1401229.  
29  
30  
31  
32  
33 (11) Yang, M.; Li, Z.; Reese, M. O.; Reid, O. G.; Kim, D. H.; Siol, S.; Klein, T. R.; Yan, Y.;  
34  
35 Berry, J. J.; van Hest, M. F. Perovskite Ink with Wide Processing Window for Scalable  
36  
37 High-Efficiency Solar Cells. *Nat. Energy* **2017**, *2*, 17038.  
38  
39  
40  
41  
42 (12) Tang, S.; Deng, Y.; Zheng, X.; Bai, Y.; Fang, Y.; Dong, Q.; Wei, H.; Huang, J. Composition  
43  
44 Engineering in Doctor-Blading of Perovskite Solar Cells. *Adv. Energy Mater.* **2017**, *7*  
45  
46 (18), 1700302.  
47  
48  
49  
50 (13) Hwang, K.; Jung, Y. S.; Heo, Y. J.; Scholes, F. H.; Watkins, S. E.; Subbiah, J.; Jones, D. J.;  
51  
52 Kim, D. Y.; Vak, D. Toward Large Scale Roll-to-Roll Production of Fully Printed  
53  
54 Perovskite Solar Cells. *Adv. Mater.* **2015**, *27* (7), 1241-1247.  
55  
56

- 1  
2  
3  
4 (14) Schmidt, T. M.; Larsen-Olsen, T. T.; Carlé, J. E.; Angmo, D.; Krebs, F. C. Upscaling of  
5  
6 Perovskite Solar Cells: Fully Ambient Roll Processing of Flexible Perovskite Solar Cells  
7  
8 with Printed Back Electrodes. *Adv. Energy Mater.* **2015**, *5* (15), 1500569.  
9  
10  
11  
12 (15) He, M.; Li, B.; Cui, X.; Jiang, B.; He, Y.; Chen, Y.; O'Neil, D.; Szymanski, P.; Eisayed, M.  
13  
14 A.; Huang, J. Meniscus-Assisted Solution Printing of Large-Grained Perovskite Films for  
15  
16 High-Efficiency Solar Cells. *Nat. Commu.* **2017**, *8*, 16045.  
17  
18  
19  
20 (16) Barrows, A. T.; Pearson, A. J.; Chan, K. K.; Dunbar, A. D. F.; Buckley, A. R.; Lidzey, D.  
21  
22 G. Efficient Planar Heterojunction Mixed-Halide Perovskite Solar Cells Deposited Via  
23  
24 Spray-Deposition. *Energy Environ. Sci.* **2014**, *7* (9), 2944-2950.  
25  
26  
27  
28 (17) Das, S.; Yang, B.; Gu, G.; Joshi, P. C.; Ivanov, I. N.; Rouleau, C. M.; Aytug, T.; Geohegan,  
29  
30 D. B.; Xiao, K. High-Performance Flexible Perovskite Solar Cells by Using a Combination  
31  
32 of Ultrasonic Spray-Coating and Low Thermal Budget Photonic Curing. *ACS Photon.* **2015**,  
33  
34 *2* (6), 680-686.  
35  
36  
37  
38 (18) Huang, H.; Shi, J.; Zhu, L.; Li, D.; Luo, Y.; Meng, Q. Two-Step Ultrasonic Spray Deposition  
39  
40 of  $\text{CH}_3\text{NH}_3\text{PbI}_{3-x}\text{Cl}_x$  for Efficient and Large-Area Perovskite Solar Cell. *Nano Energy* **2016**,  
41  
42 *27*, 352-358.  
43  
44  
45 (19) Mohamad, D. K.; Griffin, J.; Bracher, C.; Barrows, A. T.; Lidzey, D. G. Spray-Cast  
46  
47 Multilayer Organometal Perovskite Solar Cells Fabricated in Air. *Adv. Energy Mater.* **2016**,  
48  
49 *6* (22), 1600994.  
50  
51  
52  
53  
54  
55  
56

- 1  
2  
3  
4 (20) Jin, H. H.; Lee, M.; Min, H. J.; Sang, H. I. Highly Efficient  $\text{CH}_3\text{NH}_3\text{PbI}_{3-x}\text{Cl}_x$  Mixed Halide  
5  
6 Perovskite Solar Cells Prepared by Re-Dissolution and Crystal Grain Growth Via Spray  
7  
8 Coating. *J. Mater. Chem. A* **2016**, *4* (45), 17636-17642.  
9  
10  
11  
12 (21) Bishop, J. E.; Mohamad, D. K.; Wong-Stringer, M.; Smith, A.; Lidzey, D. G. Spray-Cast  
13  
14 Multilayer Perovskite Solar Cells with an Active-Area of  $1.5 \text{ cm}^2$ . *Sci. Rep.* **2017**, *7* (1),  
15  
16 7962.  
17  
18  
19  
20  
21 (22) Peng, X.; Yuan, J.; Shen, S.; Gao, M.; Chesman, A. S. R.; Yin, H.; Cheng, J.; Zhang, Q.;  
22  
23 Angmo, D. Perovskite and Organic Solar Cells Fabricated by Inkjet Printing: Progress and  
24  
25 Prospects. *Adv. Funct. Mater.* **2017**, *27* (41), 1703704.  
26  
27  
28  
29  
30 (23) Wei, Z.; Chen, H.; Yan, K.; Yang, S. Inkjet Printing and Instant Chemical Transformation  
31  
32 of a  $\text{CH}_3\text{NH}_3\text{PbI}_3$ /Nanocarbon Electrode and Interface for Planar Perovskite Solar Cells.  
33  
34 *Angew. Chem.* **2014**, *53* (48), 13239-13243.  
35  
36  
37  
38  
39 (24) Hashmi, S. G.; Martineau, D.; Li, X.; Ozkan, M.; Tiihonen, A.; Dar, M. I.; Sarikka, T.;  
40  
41 Zakeeruddin, S. M.; Paltakari, J.; Lund, P. D. Air Processed Inkjet Infiltrated Carbon Based  
42  
43 Printed Perovskite Solar Cells with High Stability and Reproducibility. *Adv. Mater. Technol.*  
44  
45 **2017**, *2* (1), 1600183.  
46  
47  
48  
49  
50 (25) Hu, Y.; Si, S.; Mei, A.; Rong, Y.; Liu, H.; Li, X.; Han, H. Stable Large-Area ( $10 \times 10 \text{ cm}^2$ )  
51  
52 Printable Mesoscopic Perovskite Module Exceeding 10% Efficiency. *Solar RRL* **2017**, *1* (2),  
53  
54 1600019.  
55  
56

- 1  
2  
3  
4 (26) Cui, X. P.; Jiang, K. J.; Huang, J. H.; Zhou, X. Q.; Su, M. J.; Li, S. G.; Zhang, Q. Q.; Yang,  
5  
6 L. M.; Song, Y. L. Electrodeposition of Pbo and Its in Situ Conversion to CH<sub>3</sub>NH<sub>3</sub>PbI<sub>3</sub> for  
7  
8 Mesoscopic Perovskite Solar Cells. *Chem. Commun.* **2015**, *51* (8), 1457.  
9  
10  
11  
12 (27) Huang, J.; Jiang, K.; Cui, X.; Zhang, Q.; Meng, G.; Su, M.; Yang, L.; Song, Y. Direct  
13  
14 Conversion of CH<sub>3</sub>NH<sub>3</sub>PbI<sub>3</sub> from Electrodeposited Pbo for Highly Efficient Planar  
15  
16 Perovskite Solar Cells. *Sci. Rep.* **2015**, *5*, 15889.  
17  
18  
19  
20  
21 (28) Koza, J. A.; Hill, J. C.; Demster, A. C.; Switzer, J. A. Epitaxial Electrodeposition of  
22  
23 Methylammonium Lead Iodide Perovskites. *Chem. Mater.* **2015**, *28* (1), 399-405.  
24  
25  
26  
27 (29) Chen, H.; Wei, Z.; Zheng, X.; Yang, S. A Scalable Electrodeposition Route to the Low-Cost,  
28  
29 Versatile and Controllable Fabrication of Perovskite Solar Cells. *Nano Energy* **2015**, *15*,  
30  
31 216-226.  
32  
33  
34  
35  
36 (30) Zhou, F.; Liu, H.; Wang, X.; Shen, W. Fast and Controllable Electric-Field-Assisted  
37  
38 Reactive Deposited Stable and Annealing-Free Perovskite toward Applicable High-  
39  
40 Performance Solar Cells. *Adv. Funct. Mater.* **2017**, *27* (11), 1606156.  
41  
42  
43  
44 (31) Potekaev, A. I.; Lysak, I. A.; Malinovskaya, T. D.; Lysak, G. V. Coatings Based on  
45  
46 Nanodispersed Oxide Materials Produced by the Method of Pneumatic Spraying. *Russ. Phys.*  
47  
48 *J.* **2018**, *60* (11), 2047-2049.  
49  
50  
51  
52  
53  
54  
55  
56  
57  
58  
59  
60

- 1  
2  
3  
4 (32) Untila, G. G.; Kost, T. N.; Chebotareva, A. B. Fluorine- and Tin-Doped Indium Oxide Films  
5  
6 Grown by Ultrasonic Spray Pyrolysis: Characterization and Application in Bifacial Silicon  
7  
8 Concentrator Solar Cells. *Solar Energy* **2018**, *159*, 173-185.  
9  
10  
11  
12 (33) Ulicna, S., Dou, B., Kim, D. H., Zhu, K., Walls, J. M., Bowers, J. W., & van Hest, M. F.  
13  
14 Scalable deposition of high-efficiency perovskite solar cells by spray-coating. *ACS Appl.*  
15  
16 *Energy Mater.* **2018**, *1*(5), 1853-1857.  
17  
18  
19  
20 (34) Huang, F.; Dkhissi, Y.; Huang, W.; Xiao, M.; Benesperi, I.; Rubanov, S.; Zhu, Y.; Lin, X.;  
21  
22 Jiang, L.; Zhou, Y. Gas-Assisted Preparation of Lead Iodide Perovskite Films Consisting of  
23  
24 a Monolayer of Single Crystalline Grains for High Efficiency Planar Solar Cells. *Nano*  
25  
26 *Energy* **2014**, *10*, 10-18.  
27  
28  
29  
30 (35) Song, S.; Hörantner, M. T.; Choi, K.; Snaith, H. J.; Park, T. Inducing Swift Nucleation  
31  
32 Morphology Control for Efficient Planar Perovskite Solar Cells by Hot-Air Quenching. *J.*  
33  
34 *Mater. Chem. A* **2016**, *5* (8), 3812-3818.  
35  
36  
37  
38 (36) Conings, B.; Babayigit, A.; Klug, M. T.; Bai, S.; Gauquelin, N.; Sakai, N.; Wang, J. T.;  
39  
40 Verbeeck, J.; Boyen, H. G.; Snaith, H. J. A Universal Deposition Protocol for Planar  
41  
42 Heterojunction Solar Cells with High Efficiency Based on Hybrid Lead Halide Perovskite  
43  
44 Families. *Adv. Mater.* **2016**, *28* (48)10701-10709.  
45  
46  
47  
48 (37) Park, B. W., Philippe, B., Gustafsson, T., Sveinbjörnsson, K., Hagfeldt, A., Johansson, E.  
49  
50 M., & Boschloo, G. Enhanced Crystallinity in Organic–inorganic Lead Halide Perovskites  
51  
52  
53  
54  
55  
56  
57  
58  
59  
60

- 1  
2  
3  
4 on Mesoporous TiO<sub>2</sub> via Disorder–order Phase Transition. *Chem. Mater.* **2014**, 26.15, 4466-  
5  
6 4471.  
7  
8  
9  
10 (38) Bu, T., Li, J., Zheng, F., Chen, W., Wen, X., Ku, Z., Peng Y., Zhong J. Cheng Y., Huang,  
11  
12 F. Universal passivation strategy to slot-die printed SnO<sub>2</sub> for hysteresis-free efficient  
13  
14 flexible perovskite solar module. *Nat. Commun.* **2018**, 9(1), 4609.  
15  
16  
17 (39) Dong, Q., Fang, Y., Shao, Y., Mulligan, P., Qiu, J., Cao, L., Huang, J. Electron-hole  
18  
19 diffusion lengths > 175 μm in solution grown CH<sub>3</sub>NH<sub>3</sub>PbI<sub>3</sub> single crystals. *Science* **2015**,  
20  
21 aaa5760.  
22  
23  
24 (40) Correa Baena, J. P.; Steier, L.; Tress, W.; Saliba, M.; Neutzner, S.; Matsui, T.; Giordano, F.;  
25  
26 Jacobsson, T. J.; Srimath Kandada, A. R.; Zakeeruddin, S. M.; Petrozza, A.; Abate, A.;  
27  
28 Nazeeruddin, M. K.; Gratzel, M.; Hagfeldt, A. Highly Efficient Planar Perovskite Solar  
29  
30 Cells Through Band Alignment Engineering. *Energy Environ. Sci.* **2015**, 8, 2928–2934.  
31  
32  
33 (41) Snaith, H. J.; Abate, A.; Ball, J. M.; Eperon, G. E.; Leijtens, T.; Noel, N. K.; Stranks, S. D.;  
34  
35 Wang, J. T.-W.; Wojciechowski, K.; Zhang, W. Anomalous Hysteresis in Perovskite Solar  
36  
37 Cells. *J. Phys. Chem. Lett.* **2014**, 5, 1511–1515.  
38  
39  
40 (42) Yang, M.; Li, Z.; Reese, M. O.; Reid, O. G.; Kim, D. H.; Siol, S.; Klein, T. R.; Yan, Y.;  
41  
42 Berry, J. J.; van Hest, M. F. A. M.; Zhu, K. Perovskite Ink with Wide Processing Window  
43  
44 for Scalable High Efficiency Solar Cells. *Nature Energy* **2017**, 2, 17038.  
45  
46  
47  
48  
49  
50  
51  
52  
53  
54  
55  
56  
57  
58  
59  
60

## Table of Contents (TOC)

